ISSN 1063-780X, Plasma Physics Reports, 2007, Vol. 33, No. 9, pp. 733–745. © Pleiades Publishing, Ltd., 2007.
Original Russian Text © A.F. Aleksandrov, K.V. Vavilin, E.A. Kral'kina, V.B. Pavlov, A.A. Rukhadze, 2007, published in Fizika Plazmy, 2007, Vol. 33, No. 9, pp. 802–815.

LOW-TEMPERATURE PLASMA

Properties of a Low-Pressure Inductive RF Discharge I: Experiment

A. F. Aleksandrov[a], K. V. Vavilin[a], E. A. Kral'kina[a], V. B. Pavlov[a], and A. A. Rukhadze[b]

[a]*Moscow State University, Leninskie gory, Moscow, 119992 Russia*

[b]*Prokhorov Institute of General Physics, Russian Academy of Sciences, ul. Vavilova 38, Moscow, 119991 Russia*

Received December 26, 2006; in final form, February 20, 2007

Abstract—Results are presented from experimental studies of low-pressure inductive RF discharges (including those with a capacitive component) employed in plasma technology. It is shown that both the RF power absorbed in the plasma and the electron density depend nonmonotonically on the external magnetic field. Discharge disruptions occurring at critical values of the magnetic field and the spatial redistribution and hysteresis of the plasma parameters were observed when varying the magnetic field and RF generator power. The parameters of the plasma of low-pressure (0.5–5 mTorr) inductive RF discharges were investigated, and the discharge properties related to the redistribution of the RF generator power between the plasma and the discharge external circuit were revealed. The experiments were performed with both conventional unmagnetized inductive plasma sources and plasma sources with a magnetic field.

PACS numbers: 52.80.Pi

DOI: 10.1134/S1063780X07090048

1. INTRODUCTION

Over the few past decades, inductive RF plasma reactors and low-pressure ion sources have been widely used in ground-based and space technologies. The main advantages of inductive RF discharges due to which they have received wide application in engineering are the possibility of achieving high electron densities at relatively low RF powers, no contact between the plasma and metal electrodes, the relatively low electron temperature, and the low plasma potential relative to the discharge chamber wall. The development of ion-beam and plasma technologies imposes stringent requirements on the performance and parameters of ion and plasma sources and gives further impetus to the revision of concepts and improvement of plasma devices. All this requires detailed knowledge of the physical processes occurring in inductive RF discharges.

Inductive RF discharges have been known for more than a century [1]. Over this period, a great body of experimental data has been accumulated [2–6], theoretical models of the penetration of RF fields into the plasma have been developed, and mechanisms for RF power absorption have been thoroughly investigated [7–10]. Recent studies, however, have shown that the properties of actual RF discharges depend not only on the current flowing through the inductor (antenna) but also on other factors. Among those are the influence of the parasitic capacitance between the inductor and plasma and the values of the active and reactive components of the external circuit impedance.

The effect of the capacitive component on the parameters of an inductive discharge was considered in [11–13]. It is now commonly accepted [11] that, at low RF powers, an inductive discharge is ignited and operates in the capacitive mode and that, after reaching a certain critical power, it passes over to the inductive mode, which is characterized by a higher plasma density than the capacitive mode. However, the effect of the capacitive component on the discharge operating in the inductive mode has still been poorly investigated.

The role of the external circuit of an unmagnetized inductive RF discharge was most thoroughly considered in [14, 15]. Using a transformer model of an inductive RF discharge, the authors showed that the RF power supplied by the generator to the external circuit is not equal to the power absorbed in the plasma. The power is redistributed between two channels: the plasma and the active elements of the external circuit. The power lost in the external circuit is determined by the ratio between the active resistance of the external circuit and the equivalent resistance of the plasma and can comprise a significant fraction of the generator power.

In [16, 19], theoretical models for bounded low-pressure inductive plasma sources in the absence and presence of an external magnetic field were developed and expressions for the equivalent plasma resistance, which determines the RF power absorbed in the plasma, were derived. In [20, 21], systematic measurements of the equivalent resistance of low-pressure inductive plasma sources were performed and the results of measurements were compared with calcula-

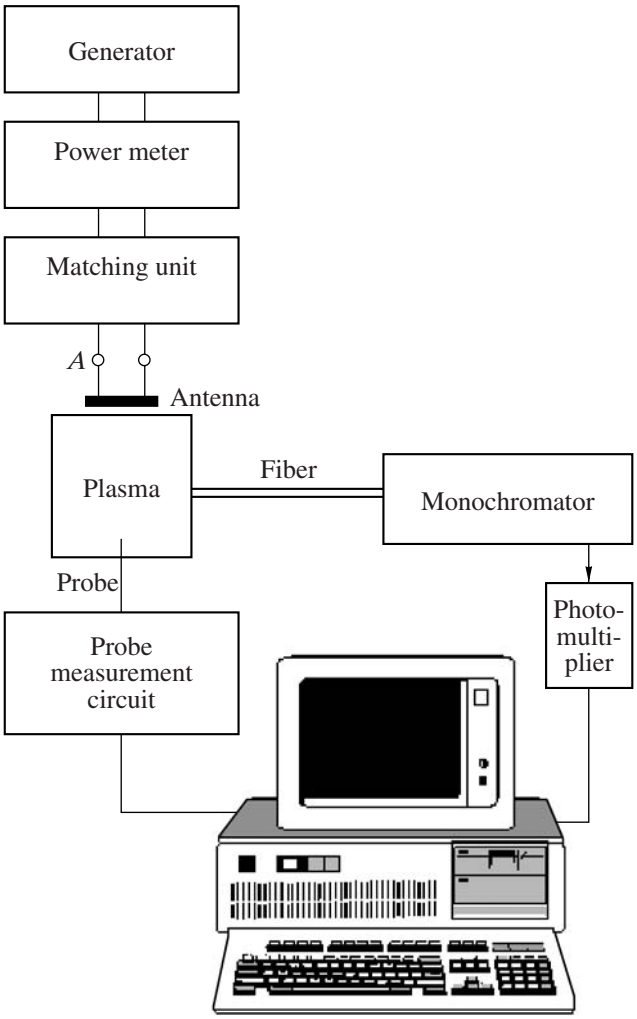

Fig. 1. Block diagram of the experimental setup.

tions [16–19]. Both theoretical and experimental results show that the efficiency of RF power absorption depends substantially on the plasma parameters, the dimensions of the plasma source, and the external magnetic field.

Computer simulations [16] show that, due to the influence of the plasma parameters on the equivalent plasma resistance, the fraction of the RF power absorbed in the plasma at a fixed resistance of the external circuit depends on the electron density, the gas pressure, the external magnetic field, and the dimensions and configuration of the plasma source. The conditions under which the plasma is matched to the RF generator depend on the same parameters [11]. In turn, the electron density and temperature depend on the fraction of the RF power absorbed in the plasma. As was shown in [16], the self-consistent redistribution of the RF power between the external circuit and the plasma can lead to physical effects that have been poorly investigated experimentally.

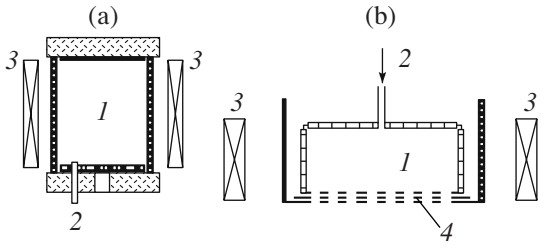

Fig. 2. Schematics of (a) a cylindrical plasma source and (b) an ion source: (*1*) discharge chamber, (*2*) gas injection, (*3*) magnetic system, and (*4*) ion-optical system.

The objective of the present work is to experimentally investigate the plasma parameters of a low-pressure (0.5–5 mTorr) inductive RF discharge (including those with a capacitive component) and to reveal its specific features related to both the power input mode and the redistribution of the RF generator power between the plasma and the external circuit. Both conventional unmagnetized inductive plasma sources and plasma sources with a magnetic field, in particular, those based on the electron cyclotron resonance [12] and on the excitation of helicons and Trivelpiece–Gold waves [22, 23], are considered. For the latter two types of sources, the effects related to the influence of the external circuit have not yet been studied.

In the second part of the work (see the present issue), the experimental results are compared to the results of computer simulations with the use of self-consistent models of a purely inductive discharge and an inductive discharge with a capacitive component.

2. EXPERIMENTAL TECHNIQUE

2.1. Experimental Setup

A block diagram of the experimental setup is shown in Fig. 1. The experiments were performed with two types of plasma sources, whose schematics are presented in Fig. 2. The first type of plasma source (Fig. 2a) was a cylindrical glass discharge chamber placed between two dielectric flanges, the inner surface of which was covered with glass. Chambers with inner diameters of 15 and 20 cm; lengths of 10, 15, 20, and 25 cm; and a wall thickness of 3 mm were used. The chamber was pumped out through special holes in the lower flange. The working gas was injected into the discharge chamber at a given flow rate through an inlet tube mounted on the lower flange, on which a metal disk serving as a reference electrode in probe measurements was also installed.

The second type of experimental device was an ion source (Fig. 2b), which consisted of a cylindrical glass discharge chamber; a gas inlet tube; a metal case; and an ion-optical system, including three perforated metal electrodes (the emitting, accelerating, and decelerating ones). In these experiments, we used discharge cham-

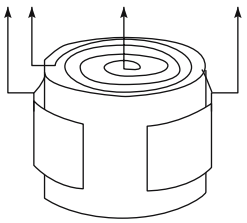

Fig. 3. Arrangement of the antenna and the capacitor at the surface of the discharge chamber.

bers with diameters of 5, 10, and 20 cm and lengths of 5, 10, 15, and 20 cm.

The magnetic field in the plasma sources was produced by solenoid magnets. The induction of the axial magnetic field inside the plasma source could be varied within the range 1–10 mT, the field inhomogeneity being about 30%.

A discharge in the plasma source was excited and maintained by inductors or antennas. Spiral antennas were mounted on the upper end surface or on the side surface of the discharge chamber (these antennas will be referred to as the end and side antennas, respectively). The antennas were made of a copper tube 3 mm in diameter and were cooled with running water. The length of the dielectric water-cooling pipes was no less than 5 m; this ensured that the resistance between the water-cooled antenna and the ground was no less than 1 MΩ.

To reduce the capacitive coupling between the antenna and plasma, metal shields with slits are usually employed [4]. However, such shields not only reduce the capacitive coupling but also suppress the inductive coupling between the antenna and plasma. In order to study how the capacitive coupling between the antenna and plasma affects the discharge characteristics, two additional capacitor plates were installed on the outer side surface of the discharge chamber (Fig. 3). The area of each plate was 25 cm^2. The plates provided a capacitive channel for power input; in this case, the inductive coupling between the antenna and plasma remained unchanged.

To excite and maintain a purely inductive discharge, the spiral antenna was connected through a matching box to an RF generator operating at a frequency of 13.56 MHz (Fig. 1). The generator power could be varied in the range 0–300 W. The power supplied to the external circuit P_{gen} was determined as the difference between the incident and reflected powers, P_F and P_R, measured by a CN-101L power meter inserted in a 50-Ω line between the RF generator and the matching unit. In our experiments, the reflected power comprised 1–10% of the incident power. For each particular set of experimental conditions, the external circuit was adjusted to match the RF generator.

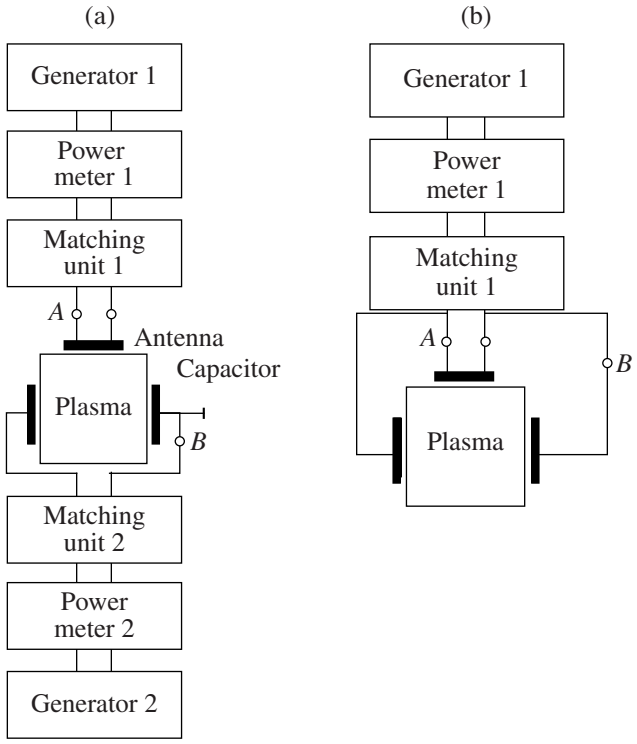

Fig. 4. Block diagram of experiments with inductive discharges with a capacitive component: (a) discharge with independent inductive and capacitive channels and (b) hybrid discharge.

To study the role of the capacitive component, the capacitor plates installed on the outer surface of the discharge chamber were connected through a separate matching unit to the second generator, whose power could be varied independently of the first generator (Fig. 4a). The second generator operated at a frequency of 13.56 MHz, and its power could be varied in the range 0–200 W. To measure the current flowing through the capacitive channel, a Rogowski coil was inserted in the circuit of the grounded electrode at point *B*. To model an actual inductive RF discharge with a capacitive component (which will further referred to as a hybrid RF discharge), an inductor was connected in parallel with a capacitor to one of the RF generators (see Fig. 4b). In this case, the currents flowing through the antenna and the capacitor were measured.

2.2. Measurements of the Power Fraction Absorbed in the Plasma

According to [16], the measured power of the RF generator was not equal to the power P_{pl} absorbed in the plasma. In order to determine P_{pl}, an RF current detector (Rogowski coil) was inserted in the circuit at point *A* (see Fig. 1). The signal from the coil was fed to either a C1-122A two-beam oscillograph or the input of an RF board of an analog-to-digital converter (ADC).

It was shown in [16] that, if the discharge was purely inductive and the load was matched to the generator, then the RF power P_{gen} supplied by the generator to the external circuit was distributed between two channels: a fraction of the power was spent on the antenna heating, while the rest of the generator power was absorbed in the plasma. The total resistive antenna losses include losses related to the heating of the antenna itself, the components of the matching unit, the metal parts of the device that are located near the plasma source and undergo the excitation of induction currents, RF connectors, etc. Taking this into account, the measurement results were processed by the following scheme.

(i) First, the effective antenna resistance in the absence of a discharge was determined by the formula

$$R_{ant} = 2P_{gen}/I_0^2, \quad (1)$$

where P_{gen} is the RF generator power supplied to the external circuit and I_0 is the antenna current in the absence of a discharge.

(ii) Then, by using the results of measurements of the antenna current and the RF generator power in the presence of a discharge, we found the total resistance of the external circuit R,

$$R = 2P_{gen}/I^2. \quad (2)$$

(iii) From the total resistance of the external circuit, the antenna resistance was subtracted to find the equivalent plasma resistance R_{pl} [16],

$$R_{pl} = 2P_{gen}/I^2 - R_{ant}. \quad (3)$$

(iv) Finally, knowing the equivalent plasma resistance, we calculated the fraction of RF power absorbed in the plasma

$$P_{pl} = 0.5R_{pl}I^2. \quad (4)$$

2.3. Probe Measurements

The plasma parameters were monitored using a set of Langmuir probes. Three probes were placed in the central cross section of the plasma source at distances of 0, 2, and 6 cm from the source axis. Each probe was a 0.3-mm-diameter tungsten wire covered with glass, except for a 5-mm-long segment at its end.

In the present work, probe measurements were performed at magnetic fields lower than 2 mT. In this case, the Larmor radius was much larger than Debye length, so no correction for the presence of the magnetic field was required. We used a standard electric circuit usually employed for such measurements. To avoid a distortion of the measured probe characteristic by the RF components of the probe current, we used resonant filters having a high resistance at the fundamental (f) and the second ($2f$) harmonics of the generator frequency. The results of measurements were processed with a computer.

The electron energy distribution function (EEDF) was calculated by doubly differentiating the probe electron current with respect to the probe potential. The effective electron temperature T_{eff} was then calculated from the known EEDFs by the formula

$$T_{eff} = \frac{2}{3}\int \varepsilon f(\varepsilon)\sqrt{\varepsilon}d\varepsilon. \quad (5)$$

2.4. Spectral Measurements

In parallel to probe measurements, we monitored the intensity of plasma radiation. Radiation from the plasma source (Fig. 1) was fed through an optical fiber onto the entrance slit of an MDR-23 monochromator, at the exit from which an FEU-100 photomultiplier was installed. The photomultiplier signal was amplified and was then recorded in a PC with the help of an ADC board. The spectrum was scanned in the wavelength range 3500–7500 Å. When measuring the spatial distribution of the plasma radiation intensity, the fiber was displaced in the radial and vertical directions. A set of apertures placed in front of the fiber allowed us to measure the radiation intensity with a spatial resolution of no worse than 2 cm.

In experiments in which the electron density was lower than 10^{11} cm^{-3}, we used an independent spectral method for determining the effective temperature of fast electrons from the intensity ratio of spectral lines. Assuming that, in our case, the plasma coronal model is applicable, the intensity ratio between two spectral lines has the form

$$\frac{I_1}{I_2} = \frac{\nu_1 \int_{eV_e}^{\infty} q_1(\varepsilon)\exp(-\varepsilon/T_e^*)\varepsilon d\varepsilon}{\nu_2 \int_{eV_e}^{\infty} q_2(\varepsilon)\exp(-\varepsilon/T_e^*)\varepsilon d\varepsilon}, \quad (6)$$

where ν_1 and ν_2 are the frequencies of the spectral lines, q_1 and q_2 are their excitation cross sections, and T_e^* is the effective temperature of fast electrons. Using the literature data [24] on the effective excitation cross sections $q(\varepsilon)$ for argon spectral lines, we calculated intensity ratio (6) as a function of the electron temperature. The obtained calibration curves are shown in Fig. 5.

The effective electron temperature was calculated from the intensity ratios of the 4191-, 4198-, and 4259-Å spectral lines to the 4200-Å line. Since the excitation cross sections for the spectral lines are known with a poor accuracy, the temperatures calculated using different lines are markedly different. The results obtained are given in the table.

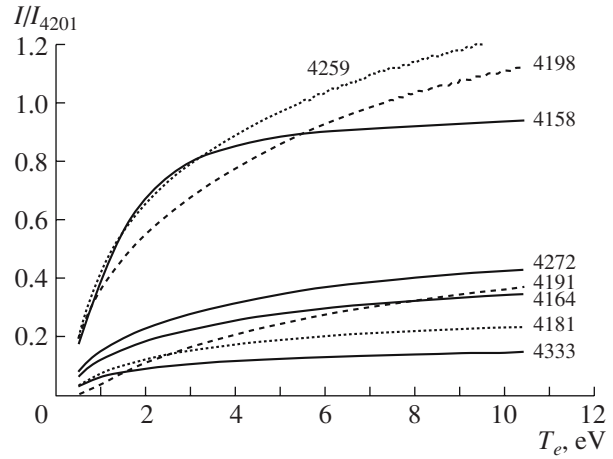

Fig. 5. Intensity I of argon lines normalized to the intensity of the Ar 4200-Å line as a function of the electron temperature T_e.

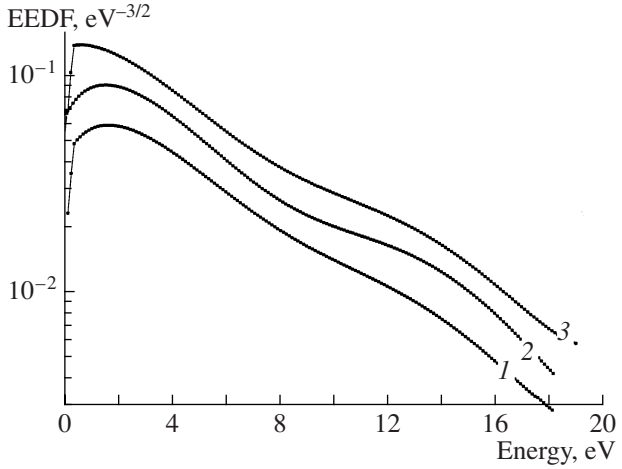

Fig. 6. EEDFs measured in the plasma of a purely inductive discharge for a magnetic field of 1.1 mT, gas pressure of 2 mTorr, and different RF generator powers: (*1*) 100, (*2*) 200, and (*3*) 300 W.

Probe measurements carried out under the same conditions showed that the EEDF was close to Maxwellian with a temperature of 4.5 eV. Comparing the temperatures determined by two different methods, one can see that the effective temperature obtained from the intensity ratio of the 4198- and 4200-Å lines is closest to that determined from probe measurements. It is the intensity ratio between these lines that was used in this study to estimate the effective electron temperature. Since the wavelengths of these lines were close to one another, we could avoid the calibration of the spectral system and could determine the I_{4198}/I_{4200} ratio without carrying out absolute measurements of the plasma radiation intensity.

The measurements were carried out in argon and xenon at pressures in the range 0.5–5 mTorr. The induction of the external magnetic field was varied in the range 0–5 mT.

3. EXPERIMENTAL RESULTS

3.1. Effect of the External Magnetic Field on the EEDF and Electron Density

Figure 6 shows typical EEDFs calculated by doubly differentiating the probe characteristics measured in the central cross section of the discharge chamber at the axis of a plasma source of radius 7.5 cm and length 10 cm. The discharge was excited by the end antenna. It can be seen that the EEDF plotted on a semilog scale has three linear segments; i.e., the EEDF in the ranges of low, moderate, and high energies is close to Maxwellian. A similar result was obtained in [4], where an inductive RF discharge in the absence of a magnetic field was investigated. It should be noted, however, that, in Fig. 6, the group of slow electrons is less pronounced than in the EEDF presented in [4]. This may be related to a change in the mechanism for electron heating in the presence of a magnetic field, because, in this case, the electron heating region is no longer localized near the chamber wall, which is inaccessible for slow electrons due to the presence of the retarding potential between the plasma and the wall. In the presence of a magnetic field, the RF electric field can penetrate deep into the plasma and can heat its internal regions.

Note that the slope of the EEDF in the range of electron energies corresponding to inelastic collisions with argon atoms is steeper than that in the range of low and moderate electron energies; i.e., the temperature T^*_{eff} of the fast electrons is lower than the temperature of the two other groups of electrons. This conclusion was confirmed by spectral measurements. Figure 7 shows the effective electron temperature T^*_{es} obtained from the slope of the probe characteristic and the temperature T^*_{eff} determined from the intensity ratio between the 4198- and 4200-Å Ar lines for different values of the magnetic field. It can be seen that the values of T^*_{eff} determined by the spectral method are systematically lower than the temperature T^*_{es} obtained from the probe characteristics.

Figures 8 and 9 show how the electron density and effective temperature at the center of the source depend on the magnetic field at different values of the RF gen-

Effective temperature of fast electrons, determined from the intensity ratio of ArI lines

I/I_{4200}	I_{4191}/I_{4200}	I_{4198}/I_{4200}	I_{4259}/I_{4200}
T_e	7.0 eV	4.6 eV	2.5 eV

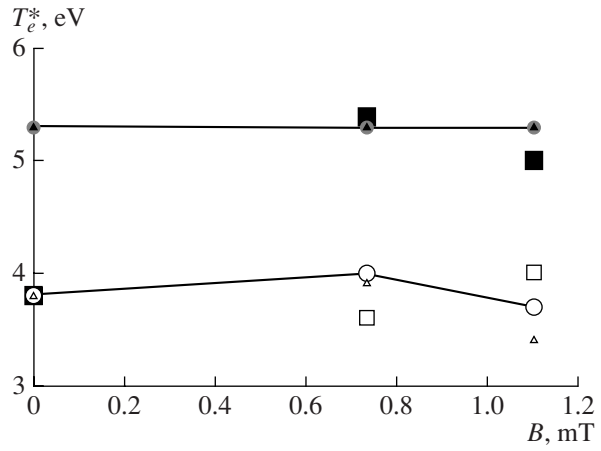

Fig. 7. Effective electron temperature as a function of the external magnetic field for an argon pressure of 2 mTorr and different RF generator powers: 100 (squares), 200 (circles), and 300 (triangles) W. The closed symbols show the temperature obtained from the slope of the probe curves, and the open symbols show the temperature determined from the intensity ratio of argon lines. The radius and length of the plasma source are 7.5 and 10 cm, respectively.

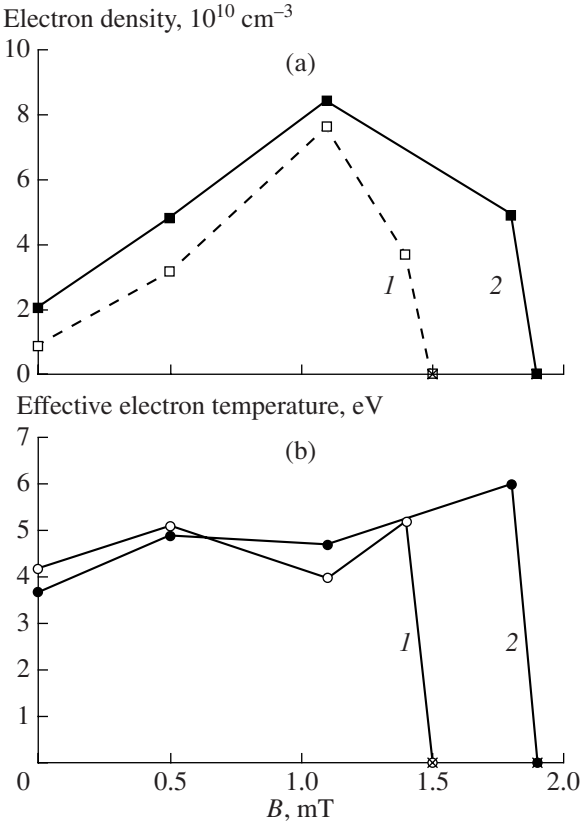

Fig. 8. (a) Electron density and (b) effective electron temperature as functions of the external magnetic field for RF generator powers of (*1*) 150 and (*2*) 200 W. The discharge disruptions are indicated by asterisks.

erator power and argon pressure. It can be seen that, in the absence of a magnetic field, the electron density is very low. As the magnetic field B increases, the plasma density first increases and, after the magnetic field reaches a certain value B_{max}, begins to decrease. When the magnetic field reaches its critical value B_{cr}, the discharge is disrupted. An increase in the RF generator power or/and gas pressure leads to an increase in the critical magnetic field B_{cr}. In contrast to the electron density, the effective electron temperature depends only slightly on the magnetic field and the RF generator power. It should be noted that the effective electron temperature somewhat increases at magnetic fields corresponding to the electron cyclotron resonance and those preceding the discharge disruption. An increase in the argon pressure leads to a decrease in the effective electron temperature.

3.2. Disruptions of an Inductive RF Discharge

Disruptions of inductive RF discharges with increasing magnetic field were also observed in previous experiments. According to [11, 12], such disruptions are caused by a mismatch between the plasma load and the RF generator because a change in the external magnetic field lead to a change in the reactive component of the plasma impedance. In our experiments, the load was matched to the RF generator for each particular value of the magnetic field, so the RF power supplied by the generator to the external circuit was fixed. However, as is seen from Figs. 8 and 9, the matching between the load and RF generator did not eliminate disruptions and did not result in the smoothing of the dependence $n_e(B)$. Moreover, our experiments showed that such disruptions are typical of inductive RF discharges in an external magnetic field over a wide range of the discharge parameters.

Figure 10 shows how the plasma radiation intensity varies with increasing magnetic field in experiments with ion sources of radius 7.5 cm and lengths 15 and 22 cm. It can be seen that the critical magnetic field B_{cr}, which limits the domain of existence of the discharge from the side of high fields, increases with increasing RF generator power and gas flow rate (i.e., gas pressure in the discharge chamber). At the same time, the second (and sometimes third) peak of the radiation intensity appears at lower magnetic fields. The domain of existence of all the peaks is bounded sharply from the side of high fields. The experiments with ion sources show that the magnetic field corresponding to the discharge disruption depends substantially on the ion extraction mode. When no voltage is applied to the ion-optical system and the ions are not extracted from the source, discharge disruptions occur at higher magnetic fields than in regimes with ion extraction (Fig. 11).

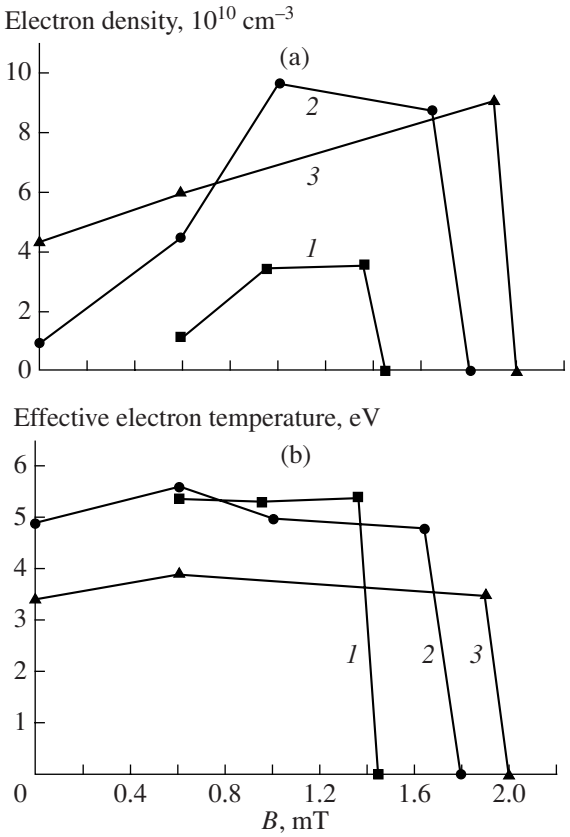

Fig. 9. (a) Electron density and (b) effective electron temperature as functions of the external magnetic field at argon pressures of (*1*) 2, (*2*) 3, and (*3*) 5 mTorr.

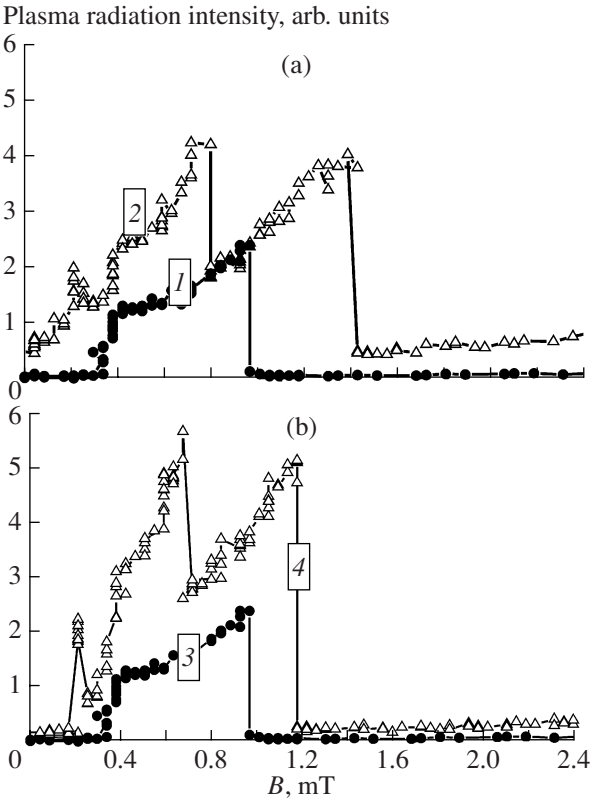

Fig. 10. Plasma radiation intensity in the central cross section of a 20-cm-diameter ion source as a function of the external magnetic field B (a) for an argon pressure of 0.5 mTorr and RF generator powers of (*1*) 300 and (*2*) 500 W and (b) for an RF generator power of 300 W and argon pressures of (*3*) 0.5 and (*4*) 1 mTorr. The discharge was excited by a spiral antenna.

3.3. Effect of the Capacitive Component on Discharge Disruptions

The results presented in the previous section were obtained in experiments with purely inductive discharges. To find out how the capacitive component of the discharge affects the dependence of the plasma parameters on the magnetic field (in particular, how it affects discharge disruptions), we carried out a series of experiments with discharges with independent inductive and capacitive channels, as well as with hybrid discharges. Figure 12 shows the measured dependences of the argon ion current on the magnetic field in an ion source with a purely inductive discharge, a discharge with independent inductive and capacitive channels, and a hybrid discharge. It can be seen that, in the purely inductive ion source, the discharge is ignited at a magnetic field of about 0.5 mT, the ion current increases with increasing magnetic field up to 1.3 mT, and the disruption occurs at a magnetic field of 1.6 mT. The situation is somewhat different when an additional power is supplied to the discharge through an independent capacitive channel. In this case, the discharge can be ignited in the absence of a magnetic field and, in the range of magnetic fields typical of disruptions of purely inductive discharges, it is not quenched but passes over to a mode typical of a purely capacitive discharge. The greater the RF power supplied through the capacitive channel and the higher the argon pressure, the smoother the transition region to the capacitive mode. In the transition region (at low magnetic fields and near the discharge disruption), the ion current in the hybrid discharge is close to that in the discharge with an independent capacitive channel at a power of 60 W. Near the peak of the ion current (at magnetic fields of 1.0–1.5 mT), the ion current in the discharge with an independent capacitive channel is somewhat higher than that in the purely inductive discharge, whereas in the hybrid discharge, the ion current is somewhat lower. It should be noted, however, that these currents differ by no more than 10–15%.

Figure 13 shows the antenna current I_{ant} as a function of the magnetic field for different types of discharge. As was expected, the difference is the largest in the transition region. Near the peak of the ion current, the values of I_{ant} in different types of discharge coincide to within measurement errors. This is quite natural because, in all these cases, the current flowing through the capacitive channel was less then 10% of the current flowing through the antenna,

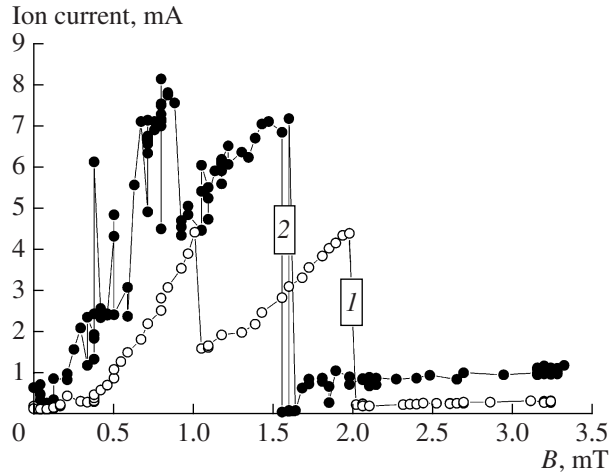

Fig. 11. Ion current to a Faraday cup located 5 cm from the ion source as a function of the magnetic field in regimes (*1*) without and (*2*) with ion extraction.

The results obtained indicate that the capacitive component of a discharge spreads out the domain of existence of a purely inductive discharge, but it only slightly affects the antenna current and the parameters of the discharge in the high-density mode.

3.4. RF Power Absorption in the Plasma of an Inductive Discharge

The fact that the electron density increases with increasing magnetic field in a purely inductive discharge can be attributed to the lower electron mobility across the magnetic field and, hence, the lower electron losses at the side wall of the plasma source. However, the decrease in the electron density with magnetic field and, the more so, discharge disruptions cannot be explained by the reduction in the electron mobility. Obviously, there are another factors affecting the discharge properties.

A possible reason for the nonmonotonic dependence of the plasma density on the magnetic field is the redistribution of the power between the antenna and the plasma with increasing external magnetic field [16]. To verify this, we determined the RF power absorbed in the plasma of a purely inductive discharge by measuring the antenna current I_{ant} at different values of the magnetic field. The results of these measurements are presented in Fig. 14. It can be seen that the initiation of a discharge leads to a slight decrease in the antenna current. As the magnetic field increases, the difference between the antenna currents in the presence and absence of a discharge increases. This indicates that the fraction of the RF generator power absorbed in the plasma increases. An increase in the magnetic field above B_{max} leads to an increase in the antenna current. After the discharge is disrupted, the antenna current returns to the value observed before the initiation of a discharge.

Figure 15 shows the RF power absorbed in the plasma as a function of the external magnetic field. The absorbed RF power was calculated from the measured values of I_{ant}. It can be seen that an increase in the magnetic field is accompanied by an increase in P_{pl}, until the magnetic field reaches the value B_{max}. Then, the

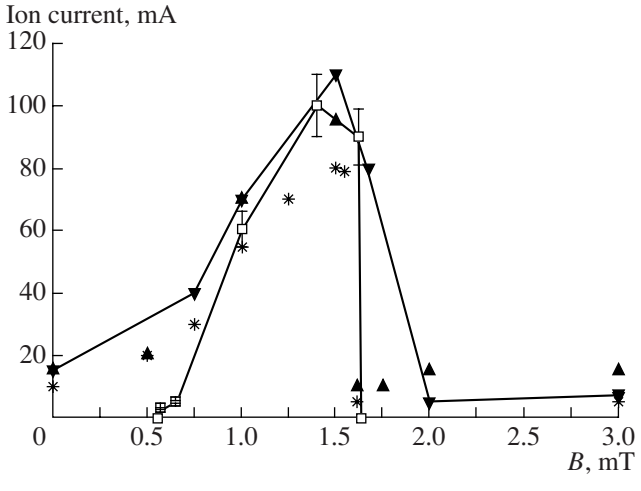

Fig. 12. Ion-beam current from an ion source of radius 5 cm and length of 10 cm as a function of the magnetic field: squares are for a purely inductive discharge; triangles with upward and downward vertices are for discharges with an independent capacitive channel, the RF generator power supplied through the capacitive channel being 60 and 200 W, respectively; and asterisks are for a hybrid discharge. The argon flow rate is 10 cm^3/min.

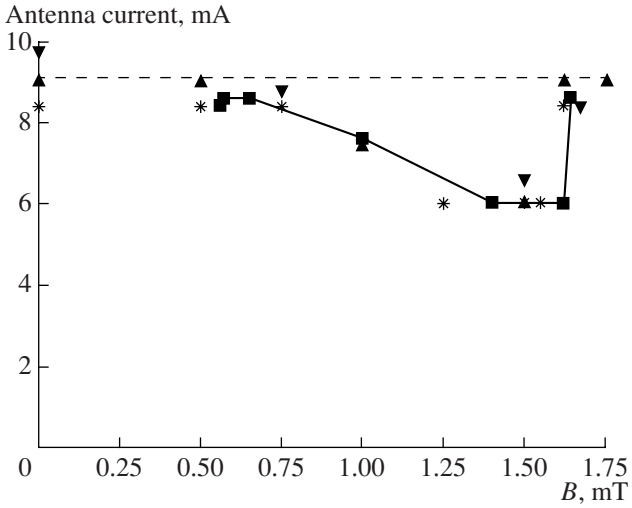

Fig. 13. Antenna current in an ion source of radius 5 cm and length of 10 cm as a function of the magnetic field: squares are for a purely inductive discharge; triangles with upward and downward vertices are for discharges with an independent capacitive channel, the RF generator power supplied through the capacitive channel being 60 and 200 W, respectively; and asterisks are for a hybrid discharge. The argon flow rate is 10 cm^3/min.

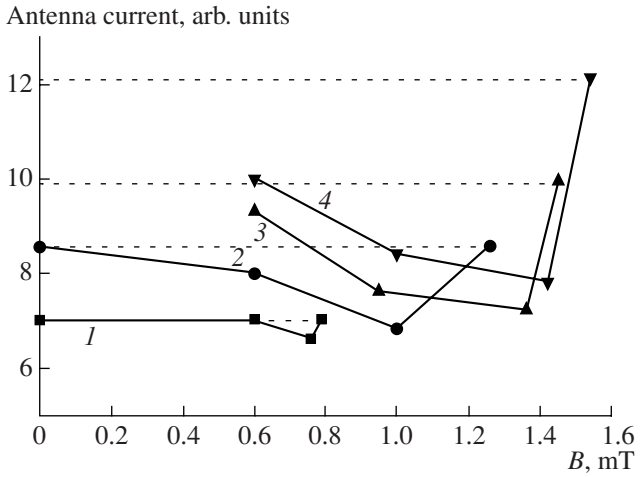

Fig. 14. Current flowing through the end antenna as a function of the magnetic field for an argon pressure of 2 mTorr and different RF generator powers: (*1*) 100, (*2*) 150, (*3*) 200, and (*4*) 300 W. The dashed lines show the antenna current in the absence of a discharge.

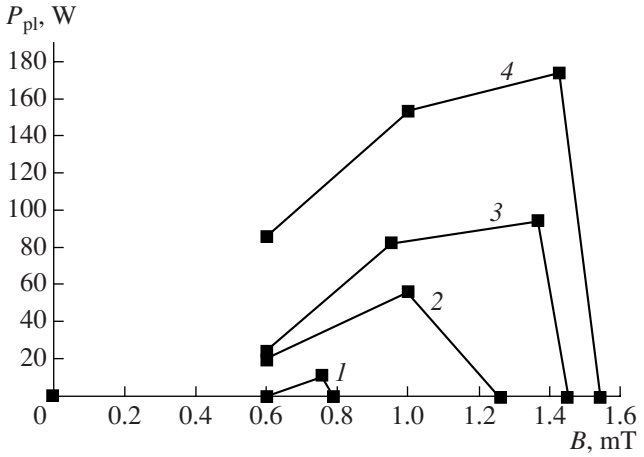

Fig. 15. Power deposited in a discharge excited by the end antenna as a function of the magnetic field for an argon pressure of 2 mTorr and different RF generator powers: (*1*) 100, (*2*) 150, (*3*) 200, and (*4*) 300 W.

power absorbed in the plasma decreases to a level that is insufficient to maintain the discharge, which is therefore disrupted.

It is interesting to compare the dependence of the RF power absorbed in the plasma on the magnetic field with a similar dependence of the electron density. The measurements showed, however, that an increase in the magnetic field was not accompanied by a proportional increase in the intensity plasma radiation in the center of the plasma source, as well as near the flanges and side wall of the source. This indicates the spatial redistribution of the plasma parameters in the source. In this case, the plasma density in different regions of the discharge depend differently on the magnetic field. Therefore, it is reasonable to study the correlation between the volume-averaged plasma density and the power absorbed in the plasma. For this purpose, we investigated the spatial redistribution of plasma parameters in the presence of a magnetic field and calculated the average plasma density.

3.5. Spatial Redistribution of the Plasma Parameters

Probe measurements show that applying an external magnetic field leads to a substantial redistribution of the plasma density $n_e(r)$, whereas the effective electron temperature changes only slightly (Fig. 16). It can be seen from Fig. 16a that, as the magnetic field increases, the electron density first increases (especially, in central regions of the discharge); then, before the disruption, the average electron density decreases, so that the local density becomes maximum in the peripheral regions of the discharge.

Figure 17 shows the radial profiles of the radiation intensity from xenon plasma sources of radius 7.5 cm and lengths of 10 and 15 cm for the cases where the discharge was excited by the end and side spiral antennas. When the magnetic field was applied to a source of length 15 cm (Fig. 17a), the radial profile of the radiation intensity initially broadened. Then, at magnetic fields corresponding to the maximum radiation intensity, the radiation intensity in the central region increased in comparison with the peripheral regions. As the magnetic field increased further, the maximum of the radiation intensity shifted toward the chamber wall. Qualitatively the same results were obtained in experiments with ion and plasma sources of radii 5 and 25 cm and lengths of 15 and 20 cm, respectively. However, for a plasma source of radius 7.5 cm and length of 10 cm, most of the power was absorbed in the peripheral regions of the plasma source over the entire range of magnetic fields under study. This effect was most pronounced when we used the side spiral antenna (see Figs. 17b–17d).

Variations in the magnetic field lead not only to the radial but also longitudinal redistribution of the plasma density. As the magnetic field increases, the longitudinal profile of the plasma radiation intensity alters. Near the antenna, the radiation intensity decreases with increasing B, whereas the distribution of the radiation intensity near the output flange varies only slightly. When the side spiral antenna is used, the relative intensity of plasma radiation from the central regions of the discharge increases with magnetic field. It should be noted, however, that the longitudinal profile of the plasma radiation intensity changes more slightly than the radial profile.

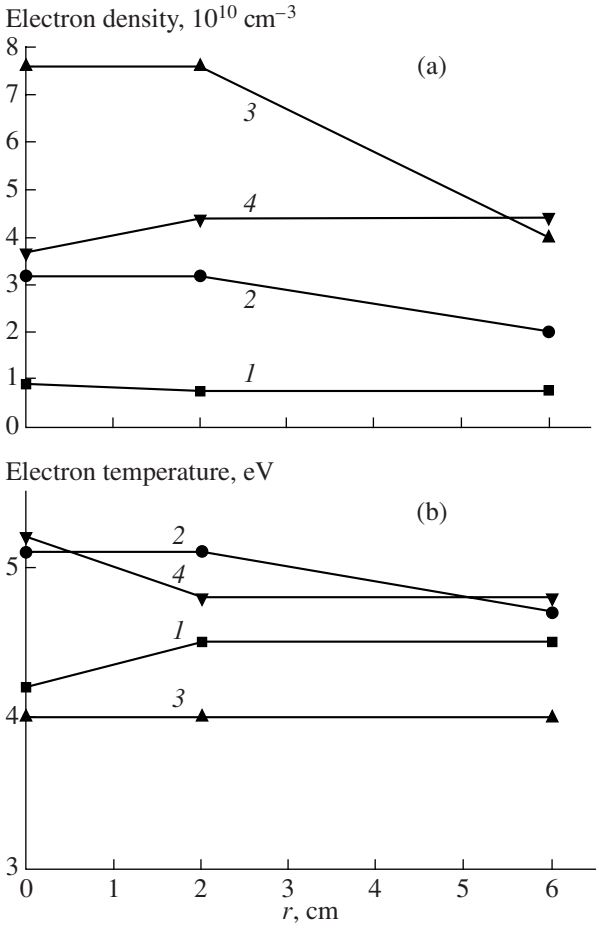

Fig. 16. (a) Electron density and (b) effective electron temperature in the plasma of an ion source of radius 7.5 cm and length of 15 cm as functions of the distance from the source axis for an RF generator power of 150 W, argon pressure of 4 mTorr, and different values of the magnetic field: (*1*) 0, (*2*) 0.5, (*3*) 1.1, and (*4*) 1.4 mT.

3.6. Effect of the Power Absorbed in the Plasma on the Average Electron Density

In order to analyze the dependence of the plasma density on the RF power absorbed in the plasma by using data of local measurements of the plasma density $n_e(r)$ in the plasma source of radius 7.5 cm and length of 15 cm, the average electron density N_e in the central cross section of the plasma source was calculated by the formula

$$N_e = \int n_e(r) r dr. \quad (7)$$

The behavior of the average electron density as a function of the magnetic field qualitatively coincides with that of the local density. First, the average density N_e increases; then, it drops and the discharge is disrupted. An increase in the RF power and gas pressure leads to an increase in the electron density and a shift of the boundary of the domain of existence of the discharge toward higher magnetic fields.

Figure 18 presents the normalized electron density $n_e/(P_{\text{pl}}p)$ (where p is the argon pressure in the discharge chamber) as a function of the power absorbed in the plasma. It can be seen that, if the power deposited in the plasma exceeds 40 W, then, within the experimental error, all the points fall on a straight line parallel to the abscissa. This means that the volume-averaged electron density in the plasma of an inductive RF discharge is proportional to the power deposited in the plasma and that the specific behavior of the plasma density as a function of the magnetic field is related to the redistribution of the RF generator power between the effective antenna resistance and the equivalent plasma resistance. An increase in the ratio $n_e/(P_{\text{pl}}p)$ at low (<40 W) input powers can be explained by the effect of the capacitive component of the discharge.

Thus, the experimental data allow us to conclude that the specific behavior of the electron density as a function of the magnetic field can be attributed to the redistribution of the RF power between two active loads: the antenna and the plasma.

3.7. Hysteresis

The results presented above were obtained at a fixed generator power under conditions such that the magnetic field was increased from zero to a value B_{fin} exceeding the value of B at which discharge was disrupted. In some experiments in which the magnetic field was first increased from zero to B_{fin} and then was again decreased to zero, we observed a hysteresis in the dependence of the plasma density on the magnetic field (Fig. 19). Measurements of the RF power absorbed in the plasma showed that, at a fixed power and certain values of the magnetic field, two regimes could occur: in the first regime, the power was almost completely absorbed in the external circuit and the plasma density was low, whereas in the second regime, the power was almost completely absorbed in the plasma and the electron density was high.

To study conditions for the appearance of hysteresis, we measured the dependence of the plasma radiation intensity on the RF generator power P_{gen} at fixed values of the magnetic field. An example of such a dependence at magnetic fields below 1 mT is presented in Fig. 20a. It can be seen that the discharge is initiated in the mode characterized by the low radiation intensity (the "low" mode). As the RF generator power is increased, the discharge passes over to the mode characterized by the high radiation intensity (the "high" mode). As the RF generator power is decreased, the power P_b at which the discharge passes over from the high to the low mode is nearly equal to the power P_f at which the discharge has passed over to the high mode when the generator power was increased. At higher magnetic fields, the situation is different (Fig. 20b). In this case, the power P_b is lower than P_f, i.e., the hysteresis occurs. The higher the magnetic field, the larger the difference between P_b and

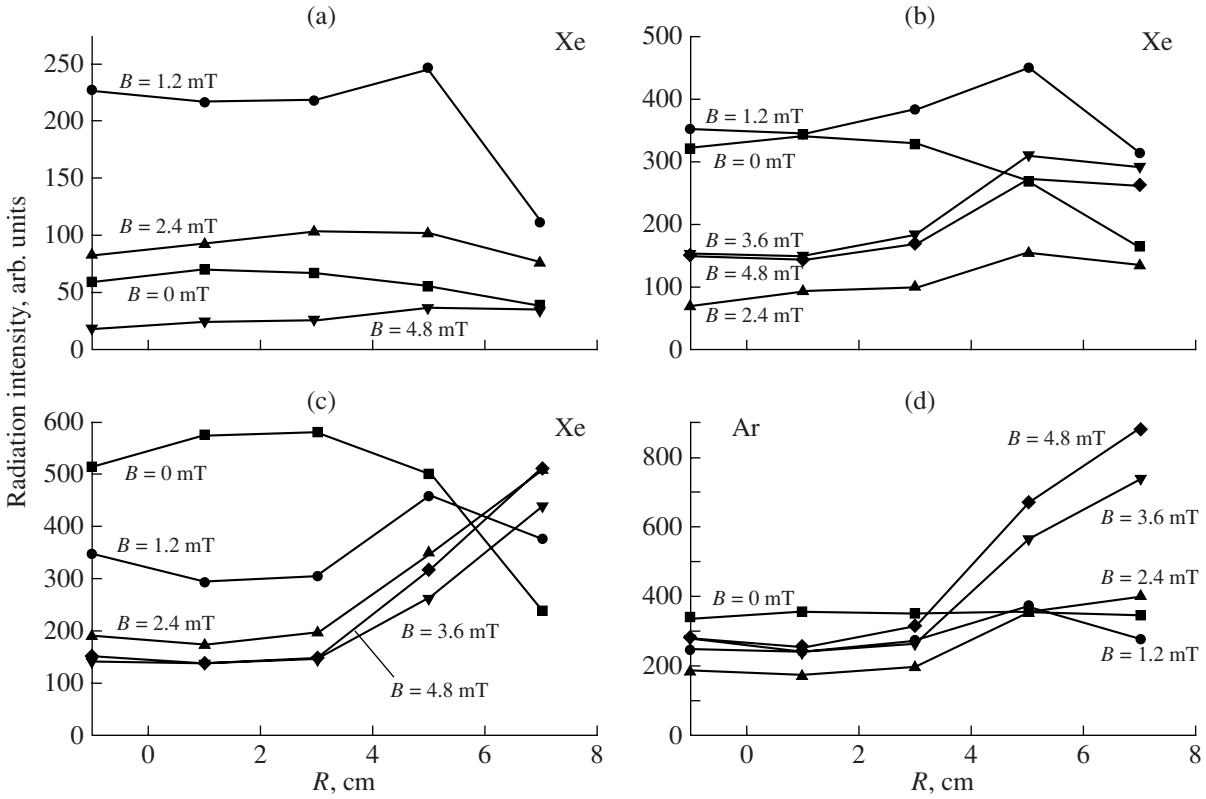

Fig. 17. Radial profiles of the plasma radiation intensity from the plasma sources of radius 7.5 cm and length of (a) 15 and (b–d) 10 cm for different values of the magnetic field. The discharges were excited by the (a, b) end (c, d) and side antennas in (a–c) xenon (the 4734-Å line) and (d) argon (the 4200-Å line).

P_f. It is worth noting that, as the magnetic field is increased, the increment in the plasma density during a transition to the high mode progressively increases. At magnetic fields above 1.4 mT, the maximum generator power (300 W) turns out to be insufficient to ensure a transition from the low to the high mode.

3.8. Effect of the Capacitive Component on Hysteresis

To find out how the capacitive component of the discharge affects the transition from the low to the high mode and back, we also performed a series of experiments with discharges with independent inductive and capacitive channels, as well as with hybrid discharges. Let us first consider the results obtained in experiments carried out without a magnetic field (Fig. 21). It can be seen that the critical inductive-channel power P_f at which the discharge passes over to the high mode is lower in the presence of the capacitive channel. The higher the fraction of the RF power supplied through the capacitive channel, the lower the power P_f and the more gradual the transition from the low to the high mode. When the antenna and the capacitor are connected in parallel, the situation is qualitatively the same, but the change in P_f is appreciably smaller. This may be explained by the power supplied through the capacitive channel being less than 100 W.

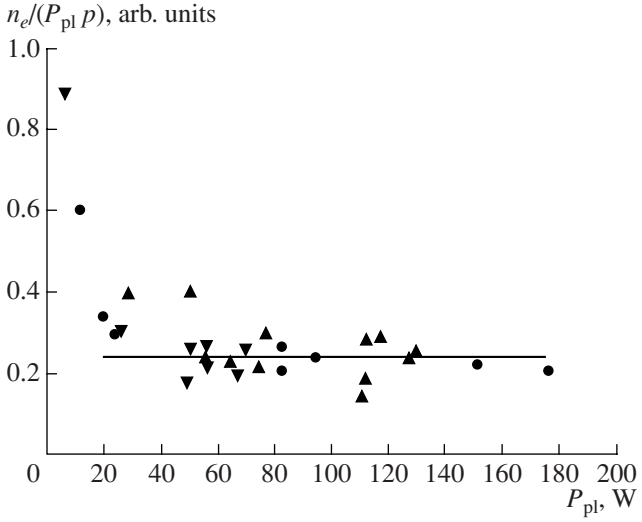

Fig. 18. Normalized electron density $n_e/(P_{pl}p)$ vs. power absorbed in the plasma.

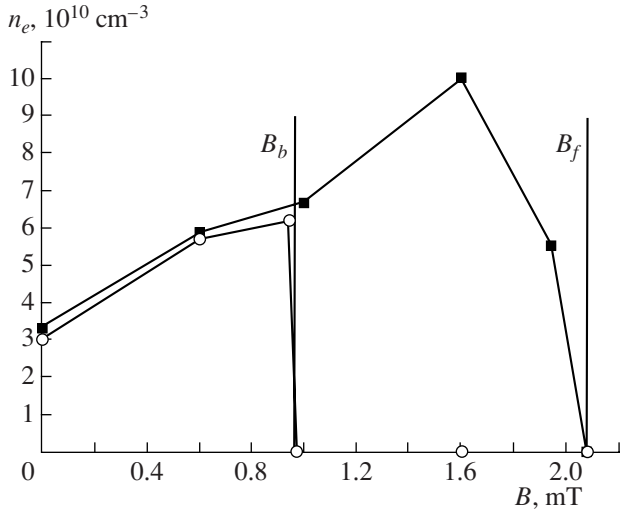

Fig. 19. Plasma density in the central cross section of the discharge chamber at the axis of the plasma source at an argon pressure of 3 mTorr and RF generator power of 200 W as a function of the magnetic field: squares and circles are for an increasing and a decreasing field B, respectively.

In the presence of an external magnetic field, the capacitive channel affects not only P_f but also P_b. It can be seen from Figs. 20c and 20d that, when the antenna and the capacitor are connected in parallel, the difference between P_f and P_b is much smaller than in the case of a purely inductive discharge, whereas in the presence of an independent capacitive channel, the difference between P_f and P_b, as well as the hysteresis effect, disappears. Hence, in the presence of the capacitive component, the discharge is more stable and the hysteresis in the dependence of the plasma parameters on the RF power and magnetic field disappears.

It is worth noting another important result that agrees with the results obtained in studying the effect of the capacitive component on the disruptions of inductive discharges in the presence of a magnetic field. When the antenna and the capacitor are connected in parallel and the discharge is in the high mode, the antenna current decreases by no more than 10% of its value in a purely inductive discharge for all of the experimental conditions under study. The plasma radiation intensity in high-mode discharges also depends

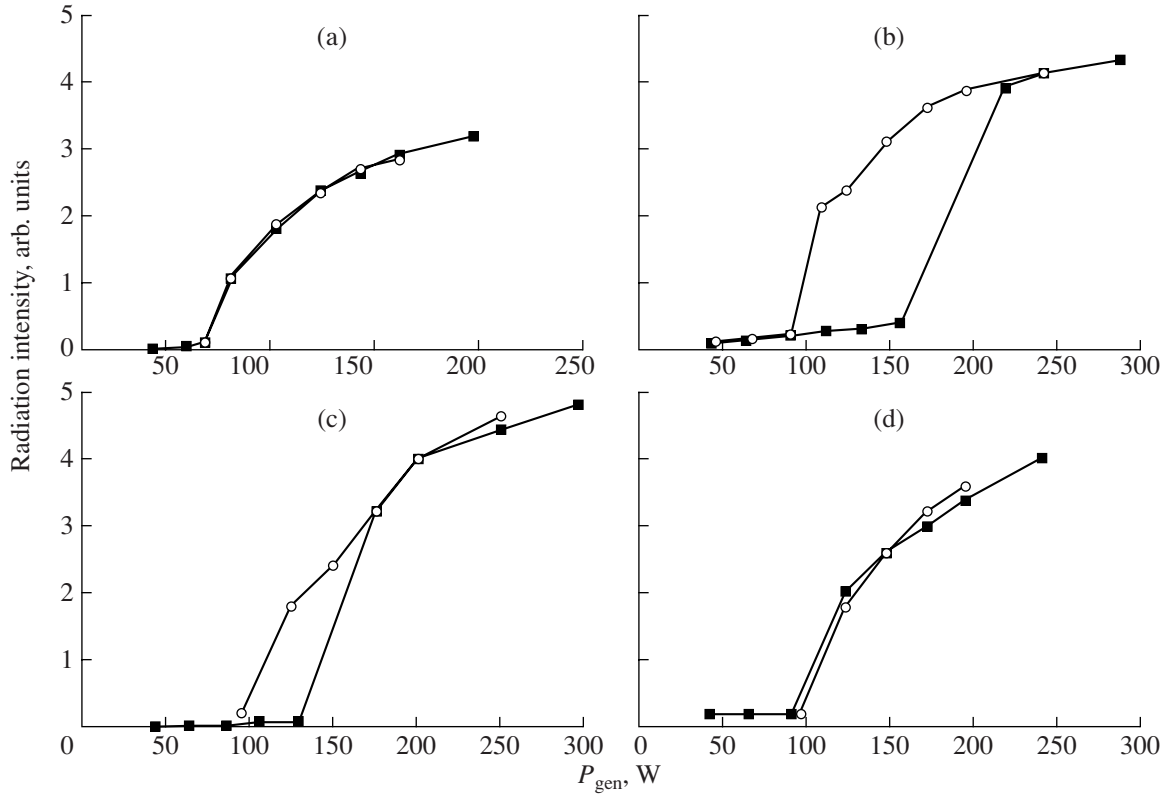

Fig. 20. Plasma radiation intensity vs. RF power supplied to the antennas of (a, b) inductive discharges excited in magnetic fields of 1 and 1.4 mT, respectively; (c) a hybrid discharge; and (d) a discharge with independent inductive and capacitive channels. The RF generator power supplied through the capacitive channel is 100 W, and the argon pressure is 2 mTorr. The squares and circles are for an increasing and a decreasing power, respectively.

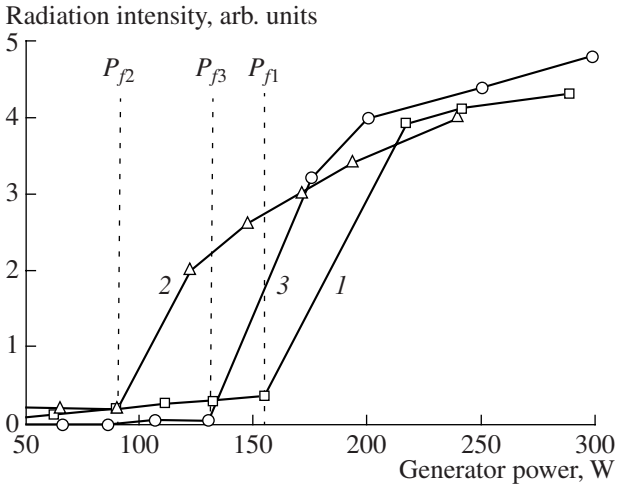

Fig. 21. Plasma radiation intensity vs. RF generator power: (*1*) purely inductive discharge excited by the end spiral antenna, (*2*) discharge with an independent capacitive channel (the RF power supplied through the capacitive channel is 100 W), and (*3*) hybrid discharge.

only slightly on the presence of the capacitive component (Fig. 21). Hence, we can conclude that the capacitive component has little effect on the discharge parameters in the high mode.

4. CONCLUSIONS

Our experiments have revealed the following specific features of a low-pressure inductive RF discharge in an external magnetic field: the electron density and the power absorbed in the plasma depend nonmonotonically on the external magnetic field; at certain critical values of the magnetic field, the discharge undergoes disruptions; and variations in the magnetic field and RF power are accompanied by the spatial redistribution of the plasma parameters, which exhibit a hysteresis effect.

In the presence of a capacitive component, the plasma parameters vary more smoothly with varying magnetic field and RF generator power, the discharge becomes more stable, and the hysteresis effect disappears.

REFERENCES

1. J. J. Thomson, Philos. Mag. **32**, 321 (1891).
2. W. Hittorf, Ann. Phys. Chem. **21**, 90 (1884).
3. V. A. Godyak, in *Proceedings of the 30th EPS Conference on Controlled Fusion and Plasma Physics, St. Petersburg, 2003.*
4. V. A. Godyak, R. B. Piejak, and B. M. Alexandrovich, Plasma Sources Sci. Technol. **11**, 525 (2002).
5. D. C. Miljak and F. F. Chen, Plasma Sources Sci. Technol. **7**, 61 (1998).
6. D. D. Blackwell and F. F. Chen, Plasma Sources Sci. Technol. **10**, 226 (2001).
7. J. Hopwood, Plasma Sources Sci. Technol. **1**, 109 (1992).
8. F. F. Chen, Plasma Phys. Controlled Fusion **33**, 339 (1991).
9. A. F. Aleksandrov, N. F. Vorob'ev, E. A. Kral'kina, et al., Zh. Tekh. Fiz. **64** (11), 53 (1994) [Tech. Phys. **39**, 1118 (1994)].
10. K. P. Shamrai and V. B. Taranov, Plasma Sources Sci. Technol. **5**, 474 (1996).
11. J. E. Stevens, in *High Density Plasma Sources: Design, Physics and Performance*, Ed. by O. A. Popov (Noyes, Park Ridge, NJ, 1996), p. 312.
12. F. F. Chen, in *High Density Plasma Sources: Design, Physics and Performance*, Ed. by O. A. Popov (Noyes, Park Ridge, NJ, 1996), p. 1.
13. R. B. Piejak, V. A. Godyak, and B. M. Alexandrovich, Plasma Sources. Sci. Technol. **1**, 179 (1992).
14. V. A. Godyak, R. B. Piejak, and B. M. Alexandrovich, Plasma Sources. Sci. Technol. **3**, 169 (1994).
15. A. F. Aleksandrov, G. É. Bugrov, K. V. Vavilin, et al., Fiz. Plazmy **30**, 434 (2004) [Plasma Phys. Rep. **30**, 398 (2004)].
16. K. V. Vavilin, V. Yu. Plaksin, M. Kh. Ri, and A. A. Rukhadze, Zh. Tekh. Fiz. **74** (5), 44 (2004) [Tech. Phys. **49**, 565 (2004)].
17. K. V. Vavilin, V. Yu. Plaksin, M. Kh. Ri, and A. A. Rukhadze, Zh. Tekh. Fiz. **74** (6), 25 (2004) [Tech. Phys. **49**, 686 (2004)].
18. K. V. Vavilin, A. A. Rukhadze, M. Kh. Ri, and V. Yu. Plaksin, Fiz. Plazmy **30**, 739 (2004) [Plasma Phys. Rep. **30**, 687 (2004)].
19. A. F. Aleksandrov, G. É. Bugrov, K. V. Vavilin, et al., Prikl. Fiz., No. 2, 41 (2006).
20. A. F. Aleksandrov, G. É. Bugrov, K. V. Vavilin, et al., Prikl. Fiz., No. 4, 54 (2006).
21. K. P. Shamrai, V. F. Virko, H.-O. Blom, et al., J. Vac. Sci. Technol. A **15**, 2864 (1977).
22. F. F. Chen, J. D. Evans, and G. R. Tynan, Plasma Sources Sci. Technol. **10**, 236 (2001).
23. A. F. Aleksandrov, G. É. Bugrov, K. V. Vavilin, et al., Prikl. Fiz., No. 5, 33 (2006).
24. *Effective Electron-Impact Excitation Cross Sections of Atoms and Ions*, Ed. by. Yu. M. Smirnov (Izd. Standartov, Moscow, 1989) [in Russian].

Translated by N.F. Larionova